Spectral photonic lattices with complex long-range coupling

Bryn A. Bell,[1,*] Kai Wang,[2] Alexander S. Solntsev,[2,3] Dragomir N. Neshev,[2] Andrey A. Sukhorukov,[2] and Benjamin J. Eggleton[1]

[1]Centre for Ultrahigh Bandwidth Devices for Optical Systems (CUDOS), Institute of Photonics and Optical Sciences (IPOS), School of Physics, University of Sydney, Sydney, NSW 2006, Australia

[2]Nonlinear Physics Centre, Research School of Physics and Engineering, Australian National University, Canberra, ACT 2601, Australia

[3]School of Mathematical and Physical Sciences, University of Technology Sydney, Ultimo, NSW 2007, Australia

*Corresponding author: bryn.bell@sydney.edu.au

Photonic systems such as arrays of coupled waveguides are well suited to emulating quantum mechanics with periodic lattice potentials, allowing the investigation of many physical phenomena in a convenient experimental setting. Usually, photons will "hop" only between neighboring lattice sites at a rate given by a purely real coupling coefficient, thus limiting the rich physics enabled by long-range coupling with complex coupling coefficients. Here we suggest and experimentally realize a spectral photonic lattice that can be configured to realize a wide variety of complex-valued coupling parameters over arbitrary lattice separations. In this system, a weak signal propagates across discrete frequency channels, driven by nonlinear interaction from stronger pump lasers. Our approach allows the experimental investigation of new discrete lattice physics—as an example, we demonstrate two novel instances of the discrete Talbot effect.

OCIS codes: (190.4223) Nonlinear wave mixing; (190.4370) Nonlinear optics, fibers.

Discrete lattice dynamics play an important role in various branches of physics, from condensed matter to topological photonics [1]. In spatial photonic lattices, such as an array of evanescently coupled waveguides, the interactions are usually dominated by nearest-neighbor (local) coupling, though the use of a 2D geometry can introduce next-nearest-neighbor coupling into a 1D lattice [2,3]. Longer range coupling is relevant in some electronic systems, and the addition of controlled non-local coupling provides more degrees of freedom to tailor the dispersion relation or band structure of the lattice. Spatial photonic lattices also usually have real-valued coupling coefficients. Complex-valued coupling coefficients cause waves propagating through the lattice to accumulate a momentum-direction-dependent phase that breaks time-reversal symmetry (TRS), i.e., moving from lattice site A to B imparts a different phase shift to moving from B to A. Broken TRS is of considerable importance in topological physics, but is challenging to implement in optics, requiring, for example, a periodic modulation of the lattice [4]. Photonic lattices utilizing dimensions other than space potentially allow greater freedom to realize these novel features and explore their effects; for instance, discrete spectral components of optical waves can couple to each other driven by nonlinear frequency conversion [5], photon–phonon interactions [6,7], and fast modulation [8]. Discrete spectral components have also been widely investigated in the context of parametric amplification, for instance, for frequency comb generation [9–11]. In contrast, here we aim to realize conservative dynamics with no overall amplification.

Here, we suggest and develop experimentally a tight-binding spectral photonic lattice, where lattice sites are represented by discrete frequency channels, which are coupled together by nonlinear frequency conversion. In such a system, controllable long-range and complex coupling are made possible by shaping the spectrum of the optical pump. Our scheme promises flexibility to implement different Hamiltonians with non-trivial band structures, particularly those breaking locality of coupling and TRS, opening up opportunities to experimentally investigate new physical effects in discrete lattices. As an example, we demonstrate a spectral analogue of the discrete Talbot effect, a self-repetitive imaging effect observed in diffractive systems with periodic input states [12,13]. We find two ways in which novel instances can be found that have not been possible in spatial lattices. First, displaced images can be formed such that they appear to be propagating in frequency with a particular direction, arising from the breaking of TRS by complex-valued hopping. Second, whereas previously it was thought that an image would occur only when the input was periodic every $N = 1, 2, 3, 4$, or 6 lattice sites [13], we show that altering the band structure with non-local coupling can lead to the Talbot effect occurring with other periodicities, and experimentally demonstrate the $N = 5$ case.

We consider a co-propagating signal and pump, whose spectra consist of discrete components separated in angular frequency by Ω. In a Kerr nonlinear medium, the signal can be up- or down-shifted by a multiple of Ω in a coherent conversion process known

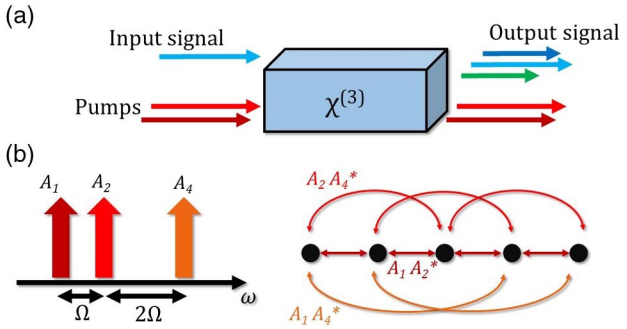

Fig. 1. (a) FWM-BS in a $\chi^{(3)}$ waveguide. A pair of pumps can up- or down-shift the signal in frequency. (b) With multiple pumps present (left), the evolution of the signal (right) is governed by multiple hopping coefficients across the lattice, depending on the amplitudes of pairs of pumps.

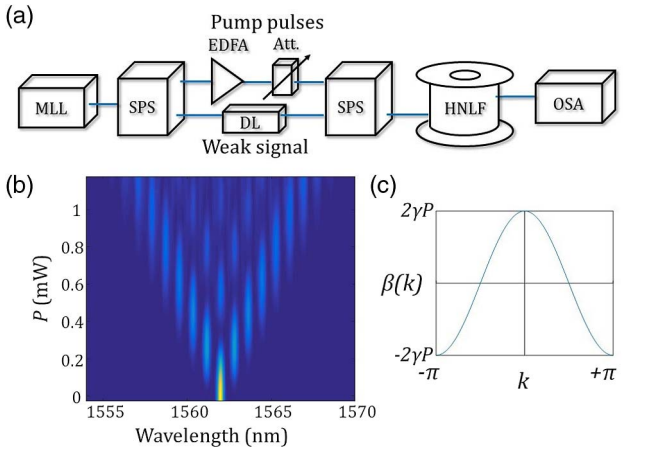

Fig. 2. (a) Experimental setup. MLL, mode-locked laser; SPS, spectral pulse shaper; EDFA, erbium-doped fiber amplifier; Att., variable attenuator; DL, tunable delay line; HNLF, highly nonlinear fiber; OSA, optical spectrum analyzer. (b) Measurement result with only two pumps. The dynamics of the evolution are apparent as the total average pump power P is varied. (c) Calculated band structure.

as four-wave mixing Bragg scattering (FWM-BS) [14], depicted in Figs. 1(a) and 1(b). FWM-BS is in principle noiseless and has attracted attention in quantum optics, for manipulating the frequency of single photons [15–19], as well as in classical communications and all-optical switching [20]. We assume that the signal and pump move at the same group velocity and group-velocity dispersion can be ignored, achieved by placing them equidistant in frequency to either side of a zero dispersion wavelength. This results in a broad phase-matched bandwidth for FWM-BS. Other nonlinear processes, such as parametric amplification of the signal by the pumps, should be phase mismatched to avoid introducing gain and noise into the signal.

The signal-envelope dynamics along propagation distance z can be described by a set of amplitudes a_n at frequency components Ωn, which evolve according to coupled-mode equations (detailed derivation is provided in Supplement 1):

$$\frac{\mathrm{d}a_n}{\mathrm{d}z} = i\sum_{j=1}^{+\infty}[c_j a_{n+j} + c_j^* a_{n-j}], \tag{1}$$

where $c_j = c_{-j}^* = 2\gamma\sum_m A_m(0)A_{m-j}^*(0)$ is the jth order coupling coefficient, γ is the effective nonlinearity, and $A_m(z)$ are the complex amplitudes of the envelope of pump spectral components.

The coupling coefficients are in general complex numbers, with a phase determined by the phases of the pumps; this can be utilized to break TRS [8]. This can be understood through the effect of couplings on the band structure of the lattice for eigenmodes $a_n(z) = \exp\{i[kn + \beta(k)z]\}$:

$$\beta(k) = \sum_{j=1}^{+\infty}[c_j e^{ijk} + c_j^* e^{-ijk}] = 2\gamma\sum_{m\neq l} A_m(0)A_l^*(0)e^{i(m-l)k}. \tag{2}$$

Here, $k = \Omega t$, and varies between $-\pi$ and π. It is surprising to see time t playing the role of wavenumber in the band structure, but this follows from treating the signal frequency as its position in the lattice, since time is the reciprocal space of frequency. In general, the pumps have differing phases and $\beta(-k) \neq \beta(k)$, which breaks TRS. Note that we are treating steady-state fields in this system, and the Schrödinger equation is written in terms of propagation z, hence the time mentioned in this context is essentially propagation distance.

The experimental setup is shown in Fig. 2(a). To produce multiple pump and signal frequencies that are mutually phase stable, a single mode-locked laser with bandwidth ~25 nm is filtered into the required frequencies using a spectral pulse shaper (SPS; Finisar WaveShaper 4000S). The pump frequencies are amplified and their power is controlled by a variable attenuator. A second SPS is used to recombine the signal and pumps while removing spontaneous emission from the amplifier, as well as to impart phase shifts to the different frequencies as required. FWM-BS occurs in a 750 m length of highly nonlinear fiber (HNLF). The HNLF has a zero dispersion wavelength at 1551 nm, so FWM-BS is well phase matched when the signal and pumps are evenly spaced to either side of this wavelength [21]. Hence, the pumps were placed around 1540 nm, with a $\Omega = 2\pi \times 100$ GHz frequency separation (~0.8 nm) between the channels, and the input signal was placed at 1562 nm. The phase-matched bandwidth for the signal is estimated to be greater than $2\pi \times 2$ THz, limited by the third-order dispersion of the HNLF.

First, we realize spectral discrete diffraction in a synthetic lattice with nearest-neighbor coupling, using two equal-amplitude pumps at neighboring spectral positions, $A_1 = A_2$. The measured spectra for this initial configuration are presented in Fig. 2(b), with the vertical axis showing increasing pump power. We note that increasing the power of all pumps uniformly increases all of the c_j uniformly, and so is equivalent to varying the time of the evolution, allowing the dynamics to be observed without the need to change the fiber length. The result shows the expected discrete diffraction pattern. In Supplement 1 we provide simulation results alongside experimental measurements showing good agreement with theory [22], and the fidelity between the measured and ideal spectrum remains >95% over the range of the evolution. Figure 2(c) shows the calculated band structure for this system, which has the usual cosine shape.

Then we implement a lattice with non-local coupling by introducing a third pump frequency, with amplitude A_4. We choose a lower power for the third component, $|A_4| \simeq 0.15|A_{1,2}|$, creating second- and third-order hopping coefficients $c_3 \simeq c_2 \simeq 0.15c_1$. The spectral evolution becomes highly dependent on the phase of this third pump, despite its lower power, as shown in

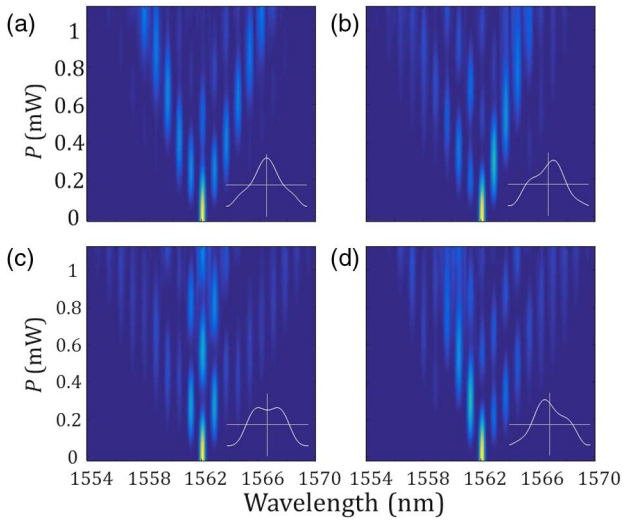

Fig. 3. Measurement results with the addition of a third pump, A_4, creating second- and third-order hopping $|c_3| \simeq |c_2| \simeq 0.15|c_1|$. The phase of the new pump is set to (a) 0, (b) $\pi/2$, (c) π, or (d) $3\pi/2$. Insets to the bottom right show calculated band structures.

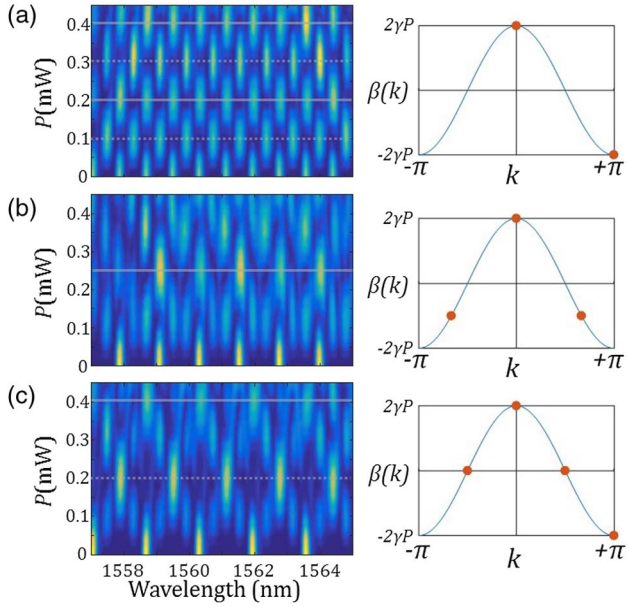

Fig. 4. Experimental demonstration of spectral discrete Talbot effect, for input signals with periodicity (a) $N = 2$, (b) $N = 3$, and (c) $N = 4$. Horizontal solid (dashed) lines mark the positions of real (displaced) images of the input. The band structures to the right of each measurement are marked with the positions of the non-zero k components in each case (orange dots).

Figs. 3(a)–3(d). For phases of 0 or π relative to the other pumps, the evolution remains symmetric, but either signal intensity can be diverted into the propagating lobes to the left and right of the diagram [Fig. 3(a)], or it can remain more localized in the central three frequency channels [Fig. 3(c)]. For phases of $\pi/2$ or for $3\pi/2$ rad [Figs. 3(b) and 3(d)], the evolution becomes asymmetric; this asymmetry is also reflected in the calculated band structure, and is connected to the breaking of TRS.

Next, we demonstrate a spectral discrete Talbot effect, where a periodic input pattern is recovered after a certain period of evolution. Whereas a discrete Talbot effect was previously demonstrated using optical waveguide arrays [13], it was fundamentally limited only to certain periodicities due to local coupling. We show how to overcome this restriction by engineering non-local coupling, enabling self-imaging of other spectral patterns.

A periodic input signal that repeats every N lattice sites contains only a discrete set of k components, $k_m = 2\pi m/N$, with m an integer such that $-\pi < k_m \leq \pi$. The corresponding eigenvalues are labeled $\beta_m = \beta(k_m)$. If the ratios of the separations between β_m are rational numbers, i.e.,

$$\frac{\beta_i - \beta_0}{\beta_j - \beta_0} = \frac{p_i}{p_j}, \tag{3}$$

where $\{p_i\}$ is a set of coprime integers, then, after some period of evolution, the separate k components will come back into phase and produce an image of the input signal. As shown in [13], for the case of nearest-neighbor hopping, this will occur only if N is in the set $\{1, 2, 3, 4, 6\}$. Initially, we realize a spectral version of the discrete Talbot effect for $N = 2, 3, 4$. Here, only two pump frequencies are used, and their separation has been decreased to $\Omega = 2\pi \times 50$ GHz ($\sim$0.4 nm), to allow more periods to fit into the useful signal bandwidth.

The simplest non-trivial case is $N = 2$ [see Fig. 4(a)]; here, the state can be described by two k components, $k = 0, \pi$. At around 0.1 mW pump power a phase difference of π has accumulated between these k components, and the input sites are depleted of signal. At around 0.2 mW, a phase difference of 2π has accumulated, creating an image, then this pattern repeats. For $N = 3$ [see Fig. 4(b)], a higher power of around 0.25 mW is required to see an image, because the allowed k components are more closely spaced in $\beta(k)$ and take longer to accumulate a 2π phase difference. The imperfections in this image could be explained by errors in setting the amplitudes and phases of the input state, or a consequence of dispersion in the nonlinear fiber. Since pulsed pumps are used, cross-phase modulation from the individual pumps causes broadening of the signal frequency channels at higher powers. Similarly, for $N = 4$, as shown in Fig. 4(c), an image can be seen at a pump power around 0.4 mW, and there is a clear displaced image at 0.2 mW.

Displaced images of the input occur when the relative phase shifts between k components are equal to an integer multiple of k. Here, a displacement of one lattice site corresponds to multiplication by a factor $\exp(ik)$ in reciprocal space. For the cases $N = 2, 4$, these displaced images can be seen in Fig. 4, occurring halfway between the real images. However, for $N = 3$, it is necessary to break TRS to obtain a displaced image. Figure 5(a) shows the $N = 3$ case, but with a $\pi/2$ phase shift applied between the two pump frequencies. This creates an asymmetric band structure where the k components for $N = 3$ lie along a straight line. The components of the state accumulate phase differences proportional to k, and hence can form an image displaced by one site at 0.15 mW pump power, then by two sites at 0.3 mW.

Previously, the discrete Talbot effect has not been demonstrated with $N = 5$ or $N \geq 7$, because when there is only nearest-neighbor hopping, these cases cannot satisfy the requirement of Eq. (3). Here, we show that by inducing non-local hopping,

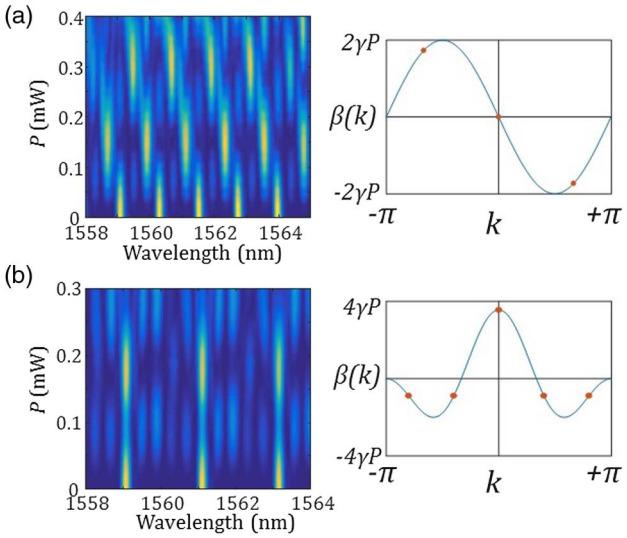

Fig. 5. (a) Talbot effect combined with image shift for $N = 3$. A $\pi/2$ phase shift between the pumps creates an asymmetric propagation in which regular displaced images appear. (b) Talbot effect for $N = 5$, which required first- and second-order couplings realized with three pump frequencies.

this restriction can be lifted. We find that for $N = 5$, the Talbot effect can be achieved by using three equally spaced pumps, $A_1 = A_3 = 2A_2$. This induces nearest-neighbor and next-nearest-neighbor hopping at equal rates, such that $\beta(k) \propto [\cos(k) + \cos(2k)]$, and

$$\beta_m = (\beta_0/4)\{-1, -1, 4, -1, -1\}, \tag{4}$$

so an image can be formed. The experimental result is shown in Fig. 5(b), and an image of the input signal is clearly seen at 0.17 mW of pump power. This approach could be extended to larger N, with long-range hopping enabling flexible band-structure engineering such that an image appears.

In future work, it should be possible to apply spectral photonic lattices to single photons and correlated photons, so as to observe quantum interference effects and entanglement. Currently Raman scattering in the nonlinear fiber generates noise, which limits single photon experiments; this could be reduced by moving the signal further from the pump in wavelength, by cooling the fiber [19], or making use of another nonlinear medium with more favorable properties.

In summary, we have demonstrated discrete spectral lattices with tunable coupling Hamiltonians enabled by the FWM-BS process. These can include non-local hopping and complex-valued coupling coefficients, by controlling the frequency separations and phases of the pump lasers. Complex-valued coupling coefficients imply a direction-dependent phase shift that breaks time-reversal symmetry and this system is in general non-reciprocal [23]. The ability to tune long-range and complex coupling coefficients provides considerable freedom to engineer the band structure, which opens possibilities to investigate new physics in lattice potentials.

Funding. Australian Research Council (ARC) (CE110001018, DP160100619, FL120100029).

REFERENCES

1. L. Lu, J. D. Joannopoulos, and M. Soljačić, Nat. Photonics **8**, 821 (2014).
2. F. Dreisow, A. Szameit, M. Heinrich, T. Pertsch, S. Nolte, and A. Tünnermann, Opt. Lett. **33**, 2689 (2008).
3. A. Szameit, R. Keil, F. Dreisow, M. Heinrich, T. Pertsch, S. Nolte, and S. Tünnermann, Opt. Lett. **34**, 2838 (2009).
4. M. C. Rechtsman, J. M. Zeuner, Y. Plotnik, Y. Lumer, D. Podolsky, F. Dreisow, S. Nolte, M. Segev, and A. Szameit, Nature **496**, 196 (2013).
5. C. Bersch, G. Onishchukov, and U. Peschel, Opt. Lett. **34**, 2372 (2009).
6. M. S. Kang, A. Nazarkin, A. Brenn, and P. St. J. Russell, Nat. Phys. **5**, 276 (2009).
7. C. Wolff, B. Stiller, B. J. Eggleton, M. J. Steel, and C. G. Poulton, New J. Phys. **19**, 023021 (2017).
8. L. Yuan, Y. Shi, and S. Fan, Opt. Lett. **41**, 741 (2016).
9. S. A. Cerqueira, Jr., J. M. Chavez Boggio, A. A. Rieznik, H. E. Hernandez-Figueroa, H. L. Fragnito, and J. C. Knight, Opt. Express **16**, 2816 (2008).
10. Y. H. Li, Y. Y. Zhao, and L. J. Wang, Opt. Lett. **37**, 3441 (2012).
11. C. J. McKinstrie and M. G. Raymer, Opt. Express **14**, 9600 (2006).
12. H. Talbot, Philos. Mag. Ser. 3 **9**, 401 (1836).
13. R. Iwanow, D. A. May-Arrioja, D. N. Christodoulides, G. I. Stegeman, Y. Min, and W. Sohler, Phys. Rev. Lett. **95**, 053902 (2005).
14. C. J. McKinstrie, J. D. Harvey, S. Radic, and M. G. Raymer, Opt. Express **13**, 9131 (2005).
15. H. J. McGuinness, M. G. Raymer, C. J. McKinstrie, and S. Radic, Phys. Rev. Lett. **105**, 093604 (2010).
16. A. S. Clark, S. Shahnia, M. J. Collins, C. Xiong, and B. J. Eggleton, Opt. Lett. **38**, 947 (2013).
17. B. A. Bell, J. He, C. Xiong, and B. J. Eggleton, Opt. Express **24**, 5235 (2016).
18. Q. Li, M. Davanço, and K. Srinivasan, Nat. Photonics **10**, 406 (2016).
19. S. Clemmen, A. Farsi, S. Ramelow, and A. L. Gaeta, Phys. Rev. Lett. **117**, 223601 (2016).
20. Y. Zhao, D. Lombardo, J. Mathews, and I. Agha, APL Photon. **2**, 026102 (2017).
21. S. Lefrancois, A. S. Clark, and B. J. Eggleton, Phys. Rev. A **91**, 013837 (2015).
22. A. Szameit, T. Pertsch, S. Nolte, A. Tünnermann, and F. Lederer, Phys. Rev. A **77**, 043804 (2008).
23. K. Wang, Y. Shi, A. S. Solntsev, S. Fan, A. A. Sukhorukov, and D. N. Neshev, Opt. Lett. **42**, 1990 (2017).